STEM CELLS TRANSLATIONAL MEDICINE®

TISSUE-SPECIFIC PROGENITOR AND STEM CELLS

Age-Dependent Effect of Pediatric Cardiac Progenitor Cells After Juvenile Heart Failure

UDIT AGARWAL,[a,b] AMANDA W. SMITH,[a,b] KRISTIN M. FRENCH,[a,b] ARCHANA V. BOOPATHY,[a,b] ALEX GEORGE,[a] DAVID TRAC,[a] MILTON E. BROWN,[a,b] MING SHEN,[c] RONG JIANG,[c] JANET D. FERNANDEZ,[d] BRIAN E. KOGON,[e] KIRK R. KANTER,[e] BAAHALDIN ALSOUFI,[e] MARY B. WAGNER,[c] MANU O. PLATT,[a] MICHAEL E. DAVIS[a,b]

Key Words. Progenitor cell • Computational biology • Pediatrics • Heart failure • Cell transplantation

[a]Wallace H. Coulter Department of Biomedical Engineering, Emory University and Georgia Institute of Technology, Atlanta, Georgia, USA; [b]Division of Cardiology and Departments of [c]Pediatrics, and [e]Cardiothoracic Surgery, School of Medicine, Emory University, Atlanta, Georgia, USA; [d]Children's Healthcare of Atlanta, Atlanta, Georgia, USA

Correspondence: Michael E. Davis, Ph.D., Department of Biomedical Engineering, Emory University, 1760 Haygood Drive, W200, Atlanta, Georgia 30322, USA. Telephone: 404-727-9858; E-Mail: michael.davis@bme.emory.edu

Received September 11, 2015; accepted for publication February 8, 2016; published Online First on May 5, 2016.

1066-5099/2016/$20.00/0

http://dx.doi.org/10.5966/sctm.2015-0241

ABSTRACT

Children with congenital heart diseases have increased morbidity and mortality, despite various surgical treatments, therefore warranting better treatment strategies. Here we investigate the role of age of human pediatric cardiac progenitor cells (hCPCs) on ventricular remodeling in a model of juvenile heart failure. hCPCs isolated from children undergoing reconstructive surgeries were divided into 3 groups based on age: neonate (1 day to 1 month), infant (1 month to 1 year), and child (1 to 5 years). Adolescent athymic rats were subjected to sham or pulmonary artery banding surgery to generate a model of right ventricular (RV) heart failure. Two weeks after surgery, hCPCs were injected in RV musculature noninvasively. Analysis of cardiac function 4 weeks post-transplantation demonstrated significantly increased tricuspid annular plane systolic excursion and RV ejection fraction and significantly decreased wall thickness and fibrosis in rats transplanted with neonatal hCPCs compared with saline-injected rats. Computational modeling and systems biology analysis were performed on arrays and gave insights into potential mechanisms at the microRNA and gene level. Mechanisms including migration and proliferation assays, as suggested by computational modeling, showed improved chemotactic and proliferative capacity of neonatal hCPCs compared with infant/child hCPCs. In vivo immunostaining further suggested increased recruitment of stem cell antigen 1-positive cells in the right ventricle. This is the first study to assess the role of hCPC age in juvenile RV heart failure. Interestingly, the reparative potential of hCPCs is age-dependent, with neonatal hCPCs exerting the maximum beneficial effect compared with infant and child hCPCs. STEM CELLS TRANSLATIONAL MEDICINE *2016;5:883–892*

SIGNIFICANCE

Stem cell therapy for children with congenital heart defects is moving forward, with several completed and ongoing clinical trials. Although there are studies showing how children differ from adults, few focus on the differences among children. This study using human cardiac progenitor cells shows age-related changes in the reparative ability of cells in a model of pediatric heart failure and uses computational and systems biology to elucidate potential mechanisms.

INTRODUCTION

Congenital heart defects (CHDs) are present in 8 of 1,000 newborns (35,000 annually), and palliative surgical therapy has greatly increased survival. Despite improved surgical outcomes, many children still develop reduced cardiac function, proceed to heart failure, and require transplantation, thus warranting better treatment options. In the past decade, multiple trials have been examined on stem cell-based therapeutics in the adult population [1, 2]; however, very few studies have been done on the pediatric population with CHDs [3]. CHDs are the leading cause of right ventricular (RV) failure in the pediatric population, especially in patients with diseases such as hypoplastic left heart syndrome and tetralogy of Fallot [4]. Surgical palliation in these patients, while being a tremendous advance, leads to an increased load on the right ventricle that is balanced by hypertrophy and fibrosis, leading to reduced cardiac function and heart failure. In fact, RV function is heavily predictive of transplant-free survival, with greatly decreased survival at RV ejection fraction (RVEF) of less than 35% [5].

Cardiac myocytes in humans were thought to be terminally differentiated cells until recently, when several studies demonstrated the capacity to self-renew the heart musculature via cardiac progenitor cells (CPCs) and other stem-like cells in the heart. Initially discovered in 2003 [6, 7], c-kit-positive CPCs have been extensively studied

in the last decade. These cells can be expanded ex vivo, making them an excellent autologous therapeutic tool for treating various heart diseases. Although these CPCs have been shown to regenerate heart tissue after myocardial infarction, few studies have been done to determine the effect on RV musculature in the pediatric population [8, 9]. c-kit$^+$ CPCs are known to exist endogenously in a dormant state and likely contribute to heart muscle regeneration when activated [10]. Despite this ability for self-renewal, the activity of CPCs is thought to decrease with age in various animal models [11, 12]. Although extensive basic and translational studies demonstrating their potential to regenerate, induce angiogenesis, improve fibrosis, and enhance endogenous responses have been done since their discovery, very few human clinical trials have been performed.

Recent clinical trials—Stem Cell Infusion in Patients with Ischemic Cardiomyopathy (SCIPIO) and Cardiosphere-Derived Autologous Stem Cells to Reverse Ventricular Dysfunction (CADUCEUS), involving CPCs and cardiosphere-like cells, respectively—have shown promising results in the adult population; however, their effects in pediatric populations still need to be explored. Published data demonstrate increased number and increased regenerative potential of hCPCs obtained from neonates [13] and that the young heart possesses more of these cells, suggesting that hCPC function in the initial newborn phase is crucial for cardiac development. A recent clinical trial demonstrated that intracoronary transplantation of autologous cardiosphere cells improved cardiac function, decreased heart failure load, and improved somatic growth in children undergoing sequential surgeries for hypoplastic left heart syndrome [14, 15] at 3 and 18 months, respectively. However, the study was performed in children with an age range of newborn to $\geq$ 3 years old. Although there have been many comparisons between cells derived from adults and children, few studies show the differences within the pediatric population. The goal of this study was to examine the effects of age of pediatric hCPCs on ventricular remodeling in juvenile RV failure and use a systems biology approach to identify potential mechanisms for age-related differences.

Materials and Methods

Human Sample Acquisition and Isolation of hCPCs

This study was approved by the Institutional Review Board at Children's Healthcare of Atlanta and Emory University. Approximately 70–100 mg of right atrial appendage tissue was obtained from children with various congenital heart diseases who were undergoing routine reconstructive heart surgeries. CPCs were isolated within 4 hours of sample acquisition. Atrial tissue was transported to the laboratory in Krebs-Ringer solution containing 35 mM NaCl, 4.75 mM KCl, 1.2 mM KH_2PO_4, 16 mM Na_2HPO_4, 134 mM sucrose, 25 mM $NaHCO_3$, 10 mM glucose, 10 mM HEPES, and 30 mM 2,3-butanedione monoxime, pH 7.4, with NaOH. Patient characteristics are described in supplemental online Table 1.

Culture and Analysis of hCPCs

Isolated cells were cultured using Hams F12 medium supplemented with 10% fetal bovine serum, 1% antibiotic and antimycotic, 1% L-glutamine, and 0.04% fibroblast growth factor 2. CPCs were passaged 3–5 times, fixed with 2% paraformaldehyde, and stained for c-kit (H-300; Santa Cruz Biotechnology, Dallas, TX, http://www.scbt.com), GATA-4 (9053; Santa Cruz Biotechnology), and Nkx-2.5 (14033; Santa Cruz Biotechnology). Both individual and pooled patient cell lines were analyzed for CPC-specific markers, as well as multidrug-resistance protein 1 (MDR-1) (8313; Santa Cruz Biotechnology) and CD34 (7324; Santa Cruz Biotechnology). Pooled cell lines were passaged 3 times, and the data were analyzed using Flow Jo V10 software.

Animal Studies

All animal experiments were performed with the approval of the Institutional Animal Care and Use Committee of Emory University. Adolescent athymic rats (Crl:NIH-*Foxn1*^{rnu}) (~150 g) were obtained from Charles River Laboratories (Wilmington, MA, http://www.criver.com). Rats were anesthetized with 2% isoflurane (Isoflurane USP; Piramal Healthcare, Boston, MA, http://www.piramel.com), orally intubated, and ventilated (Harvard Apparatus, Holliston, MA, http://www.harvardapparatus.com). A limited left thoracotomy was performed, the pulmonary trunk was exposed, and the pulmonary artery (PA) was dissected carefully from the aorta and partially ligated over an 18-gauge angiocatheter with a silk thread positioned under the PA. The catheter was removed rapidly to allow for antegrade flow through the band. Sham rats underwent the same procedure without banding the PA. Two weeks after banding, animals were randomized to treatment groups, and cells were delivered in a blinded manner.

Cell Labeling, Delivery, and In Vivo Imaging

CPCs were labeled with DiR per the manufacturer's instructions (Thermo Fisher Scientific Life Sciences, Waltham, MA, http://www.thermofisher.com). One million DiR-labeled cells were resuspended in 100 μl saline and injected in 3 areas in the RV musculature 2 weeks after banding. The rats were imaged on days 0, 3, 7, 14, and 21 using an in vivo imager (Bruker, Billerica, MA, http://www.bruker.com). The fluorescent intensity in the rat hearts caused by the DiR-labeled CPCs was quantified as percentage retention (100% on day 0) over time to account for variation in fluorescent intensity between rats.

Migration Assay

The migration assay was performed using the Boyden chamber method. In brief, 100,000 mesenchymal stem cells derived from human palate were plated on a 8-μm membrane followed by 18 hours of quiescence with no fetal bovine serum. The cells were subjected to various treatment groups for the next 18 hours. The cells were fixed with 4% paraformaldehyde and stained with 4′,6-diamidino-2-phenylindole (DAPI). Migrated cells were visualized using an IX71 microscope (Olympus, Tokyo, Japan, http://olympusamerica.com).

Proliferation Assay

The cell proliferation assay was performed using a Click-iT EdU Microplate Assay (C10214; Thermo Fisher Scientific Life Sciences). Cells were plated with growth media at 10,000 cells per well in a 96-well plate and incubated for 24 hours. 5-Ethynyl-2′-deoxyuridine (EdU) reagent was added, and the cells were incubated for an additional 24 hours. The cells were then fixed and reacted with Oregon Green 488 via a copper-catalyzed cycloaddition reaction. Anti-Oregon Green antibody conjugated with horseradish peroxidase was added and subsequently reacted with Amplex UltraRed substrate to produce a red fluorescent product. The absorbance of the samples was read with a BioTek Synergy 2 plate reader at 530/590 nm.

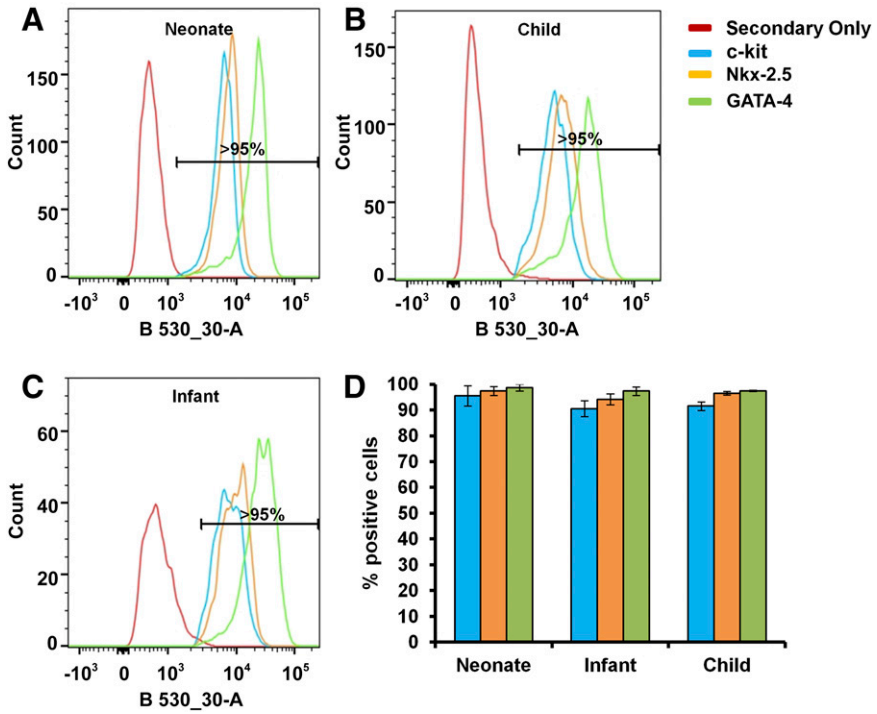

Figure 1. Characterization of human pediatric cardiac progenitor cells (hCPCs) by flow cytometric analysis of cell markers. c-kit (blue), GATA-4 (orange), and Nkx-2.5 (green) expression was determined in pooled hCPCs isolated from each age group: neonate **(A)**, child **(B)**, and infant **(C)**. **(D):** Mean ± SEM of hCPC marker expression for three passages. Abbreviation: B 530_30-A, filter for identifying Alexa Fluor 488.

Immunostaining

Rats were sacrificed at days 7 and 28 after cell injections. Hearts were harvested and fixed in formalin followed by paraffin embedding. Immunostaining was performed per the protocol. In brief, paraffin wax was removed from the 7-μm tissue sections using Histo-Clear, followed by various alcohol washes. Antigen retrieval was performed using sodium citrate followed by blocking with 3% bovine serum albumin. Tissues were incubated with primary antibodies overnight at 4°C followed by 2-hour incubation of secondary antibodies at 37°C in a humidified dark chamber. Antibodies used were rabbit anti-c-kit (1:50 dilution) (sc168; Santa Cruz Biotechnology), mouse anti-human mitochondria (1:100 dilution) (NBP2-32982; Novus Biologicals, Littleton, CO, http://www.novusbio.com), rabbit anti-rat stem cell antigen 1 (SCA-1) (1:50 dilution) (AB4336; EMD Millipore, Billerica, MA, http://www.emdmillipore.com), Isolectin GS-IB4 Alexa Fluor 647 conjugate (1:25 dilution) (Thermo Fisher Scientific Life Sciences), Alexa Fluor 488 goat anti-rabbit (1:200 dilution) (A11008; Thermo Fisher Scientific Life Sciences), Alexa Fluor 594 goat anti-mouse IgG1 (1:200 dilution) (A21125; Thermo Fisher Scientific Life Sciences), and Alexa Fluor 647 goat anti-rabbit (1:200 dilution) (A21244; Thermo Fisher Scientific Life Sciences).

Echocardiography

To evaluate heart function, echocardiography was performed on PA-banded and sham rats at 2, 4, and 6 weeks after surgery. Transthoracic echocardiography was performed by the Emory +Children's Animal Physiology Core using a Vevo 2100 digital high-frequency ultrasound system (FujiFilm Visualsonics, Toronto, ON, Canada, http://www.visualsonics.com) equipped with a probe (MS250) suited for rat imaging. RVEF was measured in short-axis view, and tricuspid annular plane systolic excursion (TAPSE) of the lateral portion was determined in apical four-chamber view in M-mode. RV wall thickness was measured in the two-dimensional long-axis parasternal view by M-mode.

Picrosirius Staining

Picrosirius staining was performed for collagen assessment. Paraffin-embedded sections were dewaxed using Histo-Clear. Multiple ethanol washes were performed in series followed by 1-hour incubation with Picrosirius solution (Sigma-Aldrich, St Louis, MO, http://www.sigmaaldrich.com). The sections were washed with acetic acid followed by ethanol and mounted with resinous medium (Cytoseal). Images were taken using a slide scanner (Hamamatsu Nanozoomer 2.0HT, https://www.hamamatsu.com). Percentage fibrosis was quantified using Aperio Imagescope v12.1.0.5029 software.

Gene and MicroRNA Array Analysis

RNA was extracted and whole gene and microRNA (miRNA) array was performed on three hCPC cell lines from three different patients in each group: neonate, infant, and child. Affymetrix gene arrays were performed by the Emory Integrated Genomics Core. Principal component (PC) analysis and partial least squares regression (PLSR) were performed using SIMCA-P software (UMetrics, Umeå, Sweden, http://umetrics.com) that solves the PLSR problem with the nonlinear partial least squares algorithm. Gene data were analyzed by Metacore and ingenuity pathway analysis.

Statistical Analysis

Statistics were calculated with GraphPad Prism software as described in the legends.

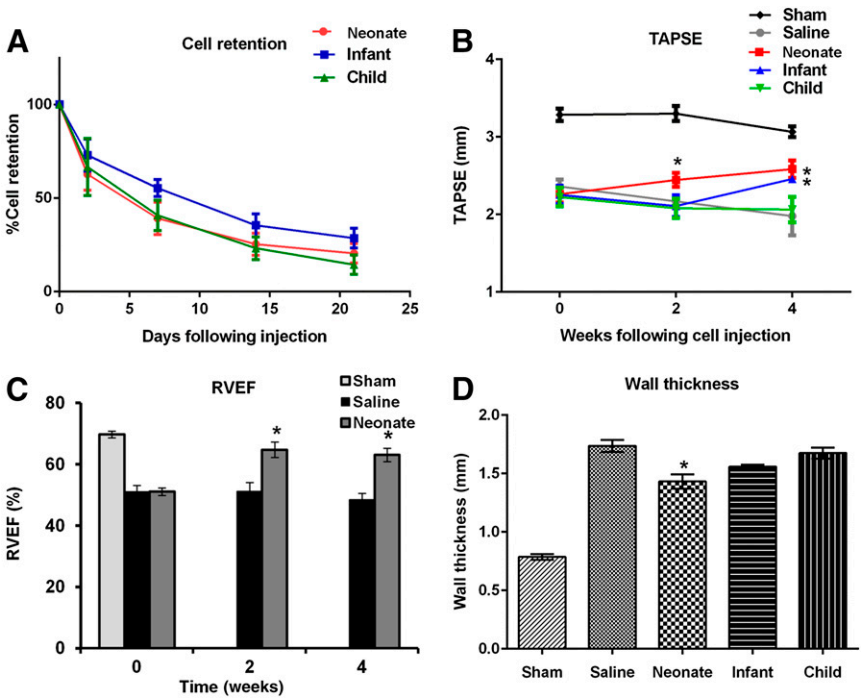

Figure 2. Cell retention and functional analysis. **(A):** Intramyocardial injection of labeled cells was followed for 21 days. Data represent mean ± SEM of fluorescence intensity at days 3, 7, 14, and 21 (n = 8–9) with no statistical difference. **(B–D):** Two-dimensional echocardiography was performed on banded rats at 2, 4, and 6 weeks after the procedure. **(B):** TAPSE (mm) was analyzed at baseline and 2 and 4 weeks after cell injection. Data represent mean ± SEM. *, $p < .05$; 2-way analysis of variance (ANOVA) with difference between newborn (n = 9) and saline (n = 4) and between infant (n = 8) and saline at the time point indicated. **(C):** RVEF was assessed at 2 and 4 weeks after human cardiac progenitor cell transplantation. Data represent mean ± SEM. *, $p < .05$; ANOVA followed by Tukey-Kramer post-test between neonate (n = 6) and saline group (n = 5). **(D):** Wall thickness (mm) was analyzed at 6 weeks after banding. Data represent mean ± SEM. *, $p < .05$; ANOVA followed by Tukey-Kramer post-test between neonate (n = 8) and saline group (n = 7). Abbreviations: RVEF, right ventricular ejection fraction; TAPSE, tricuspid annular plane systolic excursion.

RESULTS

Isolation and Characterization of hCPCs

Human CPCs were categorized in 3 different age groups (neonate, 0 days to 1 month; infant, 1 month to 1 year; and child, 1 to 5 years). To characterize the isolated cells, hCPCs were passaged 3 to 5 times and pooled from 3 individual subjects from each age group to form neonate, infant, and child hCPC cell lines. These cell lines were then subjected to 3–5 passages and identified by >90% of c-kit, Nkx-2.5, and GATA-4 expression by flow cytometric analysis, suggesting the maintenance of CPC phenotype over several passages (Fig. 1). Cells were negative for CD34 and positive for MDR (data not shown).

Age of hCPCs Does Not Affect Retention

DiR-labeled hCPCs (1 million) from each age group (neonate, infant, and child) were injected in the right ventricle of athymic rats by non-invasive, echo-guided injection 2 weeks after pulmonary artery banding (PAB). Live animal imaging was conducted at days 0, 3, 7, 14, and 21 to monitor hCPC retention and survival postinjection. More than 70% of hCPCs were retained at the site of injection on day 3, and <20% of hCPCs were retained on day 21 among all the groups (neonate [n = 9], infant [n = 7], and child [n = 8]). No statistical difference was observed between the groups at any of the time points (Fig. 2A).

CPC Efficacy on Cardiac Function and Remodeling After PAB Is Age-Dependent

Athymic rats were transplanted with 1 million hCPCs from each respective group of donor cells 2 weeks after banding, and cardiac function was followed longitudinally for 4 weeks after cell transplantation. We observed a significant decrease in RV function as measured by TAPSE and RVEF after PAB surgery. Neonate donor hCPCs showed improved RV function at 2 weeks postinjection, which was maintained at 4 weeks compared with PAB saline-treated rats. For both infant and child cells, no significant difference was present at 2 weeks after cell implantation, although at 4 weeks infant hCPC-treated animals had significantly improved TAPSE (Fig. 2B). RVEF calculated at 2 and 4 weeks after hCPC injection was significantly improved in PAB animals treated with neonate hCPCs compared with controls at both time points (Fig. 2C). No significant difference was present among groups with infant and child hCPCs (data not shown).

We assessed RV wall thickness and fibrosis as functions of remodeling 6 weeks after PAB (4 weeks after cell injection). Results demonstrate significantly decreased wall thickness (Fig. 2D) and fibrosis (Fig. 3) in neonate hCPC-treated rats compared with saline-treated rats. No significant difference was found among other groups, although strong trends were observed between infant and control groups in wall thickness and fibrosis.

Computational Modeling of miRNAs and Systems Biology of Genes

We have previously used principalPC analysis and PLSR to establish relationships between covariant miRNAs within CPC exosomes and regenerative effects [16]. Here, we used CPCs from three patients per group and performed whole miRNA and gene arrays to establish a relationship between donor CPC age (cues),

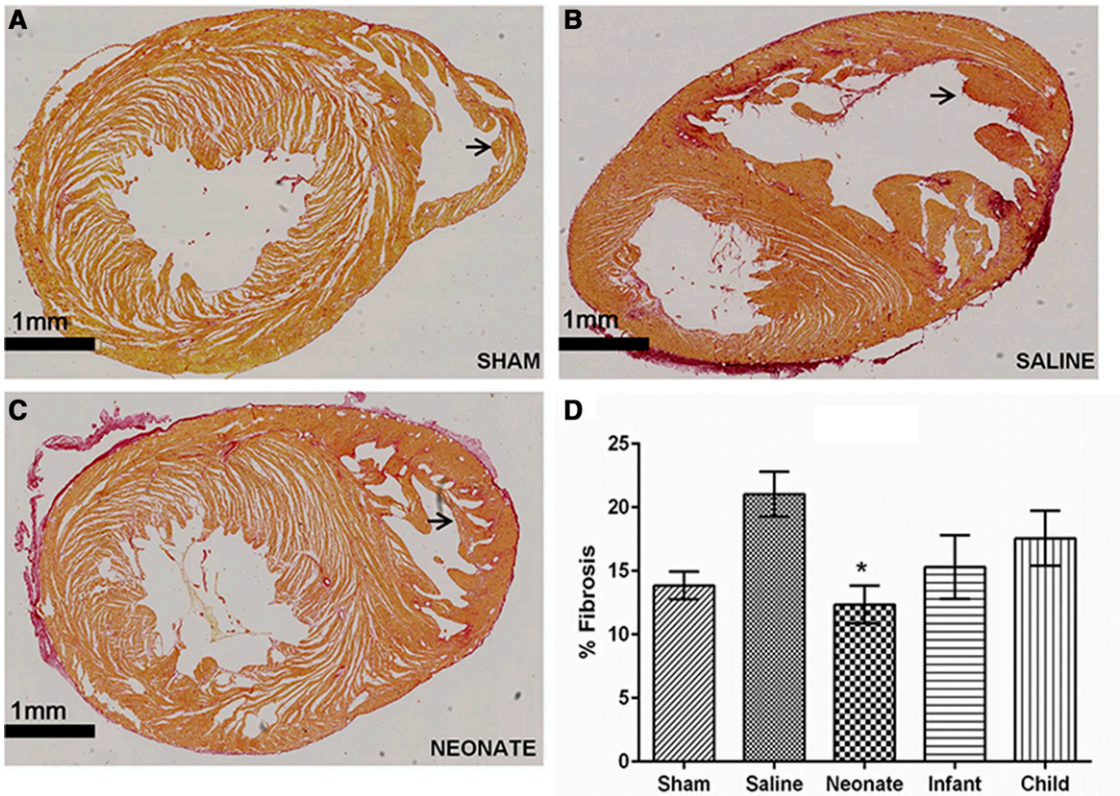

Figure 3. Fibrosis analysis. Picrosirius staining of paraffin-embedded banded hearts. Arrow indicates right ventricular wall. **(A–C):** Representative images as labeled. **(D):** Grouped data represent mean ± SEM of percentage fibrosis. ∗, $p < .05$; analysis of variance followed by Tukey-Kramer post-test; saline ($n = 3$) versus neonate human cardiac progenitor cell-transplanted peripheral artery banding rats ($n = 4$) groups.

miRNA or mRNA (signals), and responses of TAPSE, wall thickness, and fibrosis using PLSR. The scores plot illustrates tight clustering in PC space by age, even for the three distinct patients (Fig. 4A). Variable importance of projection calculations determined each miRNA signal's contribution to an outcome. We used miRTarBase to narrow the top 100 miRNAs to 29 validated miRNAs with known targets (by at least 3 assays) and plotted them in PC space with outcomes (Fig. 4B). After statistical analysis of gene array data, we used ingenuity pathway analysis to compare the miRNA targets from each group to each other and find consensus pathways strongly represented in neonate and child groups, as that is where most functional differences occurred. Figure 4C shows the pathways of the miRNA targets that differ between neonates and child donors (negative logP value on *x* axis). The mRNA microarray was also performed, and a full pathway analysis and full PLSR to identify genes that mapped to function are shown in Figure 5A and 5B, respectively. In the top 300 genes identified by PLSR analysis from mRNA microarray with the same response matrix, similar pathways were upregulated between neonate and child (Fig. 5C), and we found the strongest enrichment in neonate versus child, followed by neonate versus infant, with less enrichment in the infant-versus-child comparison (Fig. 5D).

hCPCs Transplantation Improved Angiogenesis

Computational models and pathway analysis suggested that hCPCs of all age groups possess an ability to induce angiogenesis. We analyzed this observation further and determined the degree of angiogenesis in the RV musculature of athymic rats treated with hCPCs by performing isolectin staining 28 days post-transplantation. Vessels were counted in a 20× field. We observed that hCPC intramyocardial transplantation into right ventricle showed significantly increased angiogenesis compared with the saline-only group; however, the age of hCPCs had no impact on increased angiogenesis, suggesting that the pathways involving angiogenesis are conserved in neonate, infant, and child cells (Fig. 6).

Neonate hCPCs Have the Maximum Capacity for Chemotaxis and Proliferation

We assessed the chemotactic potential of these cell types. Human mesenchymal stem cells (hMSCs) were subjected to 18 hours of quiescence and then another 18 hours of conditioned medium treatment (for each age group), and migration was measured using a modified Boyden chamber assay. Our data show a nearly 12-fold increased ability of neonate cell media to attract hMSCs compared with control media. In contrast, media from infant (5.6-fold) and child (2.6-fold) hCPCs had reduced migratory response on hMSCs (Fig. 7A).

Based again on our computational modeling data, we also examined pathways enriched in neonate hCPCs. Pathways involving cell-cycle chromosomal condensation were significantly increased in neonates, suggesting their high proliferative potential. To assess the proliferative potential of these cell types, we used an EdU incorporation assay. The results demonstrate that neonate hCPCs have the maximum capacity to proliferate, followed by infant and then child hCPCs (Fig. 7B).

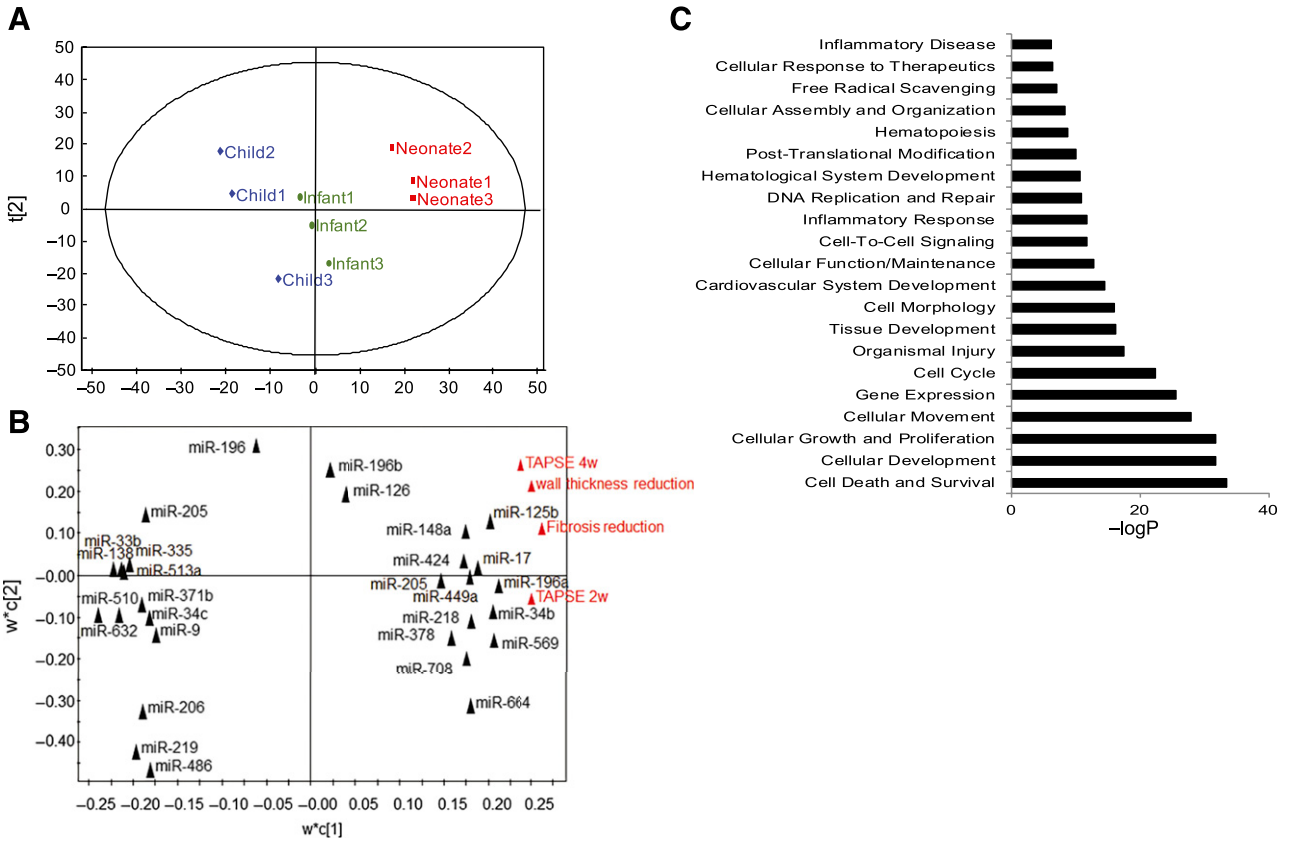

Figure 4. Computational modeling and systems biology. **(A):** Principal component analysis of patient miRNA. Patients were analyzed individually (n = 3) for microRNA (miRNA) content, and results were plotted in principal component (PC) space. Each age group clustered together despite being different patients. **(B):** Partial least squares regression analysis (PLSR) analysis of patient miRNAs and cardiac function demonstrates target-validated 29 miRNAs of top 100 that clustered with or against responses. **(C):** miRNA target analysis. PLSR identified top 100 miRNA variable importance of projections. Targets were determined using miRTarBase for validated targets, which returned 29 miRNAs. Ingenuity pathway analysis was used to determine the networks of the targets. Abbreviation: TAPSE, tricuspic annular plane systolic excursion.

We further tested the chemotactic ability of these cells in vivo. We performed SCA-1 immunostaining 7 days after c-kit and CPC transplantation. Our data suggest increased recruitment of SCA-1-positive cells to the right ventricle in treated animals compared with saline-only controls (Fig. 7C).

Discussion

The benefits of CPC therapy were initially believed to be a function of their ability to directly regenerate the myocardium. Further studies revealed that increased tissue oxygenation via angiogenesis, improved recovery of cellular and tissue function (the positive remodeling effect), and decreased native cell death (anti-apoptosis or antinecrosis) also contribute to the therapeutic efficacy of CPCs. Multiple preclinical and translational studies have been done to harvest the therapeutic potential of these cell types in adult population with ischemic insults; however, few studies have been conducted on the pediatric population [9, 14].

Multiple congenital heart defects exist in humans, and their treatment is age-dependent; thus it is critical to determine when donor cells are most effective. To address this, we used the approach of delivering hCPCs of various age groups (neonate, infant, and child) harvested from right atrial appendage to decipher the potential mechanisms and pathways responsible for improved fibrosis, hypertrophy, engraftment, and cardiac function in a juvenile RV heart failure model. Our results suggest that in animals subjected to PAB, transplantation of neonate hCPCs significantly improved remodeling and cardiac function within 2 weeks of treatment, which was maintained through 4 weeks. Although no significant acute benefit in the initial 2 weeks was observed with infant hCPCs, a significant improvement in TAPSE was observed at 4 weeks, with a strong positive trend for hypertrophy and fibrosis. Increased recruitment of SCA-1-positive cells after 7 days of cell transplantation might play a role in these observations. Moreover, these findings are in agreement with the findings published recently in an infarct model by Simpson et al. [13], who demonstrated that neonatal hCPCs are more proliferative, regenerative, and angiogenic compared with their adult counterparts, leading to improved cardiac remodeling in a myocardial infarction model. Although that study compared cells from neonates to those of adults, it did not examine other age groups within the pediatric population.

To decipher the potential mechanisms responsible for the observed findings, we took a computational and systems approach. miRNA principal component analysis revealed age-dependent clustering of the different patient-derived hCPCs despite differing diagnoses (Fig. 4A). PLSR analysis gave quantitative outputs to how likely each was to be involved in our response. Certain miRNAs handpicked in our study have been shown to regulate fibrosis (miR-17, miR-9) [17], cardiac hypertrophy (miR-378, miR-34b, miR-9) [17], and cell reprogramming (miR-206 and miR-138) [18]. After

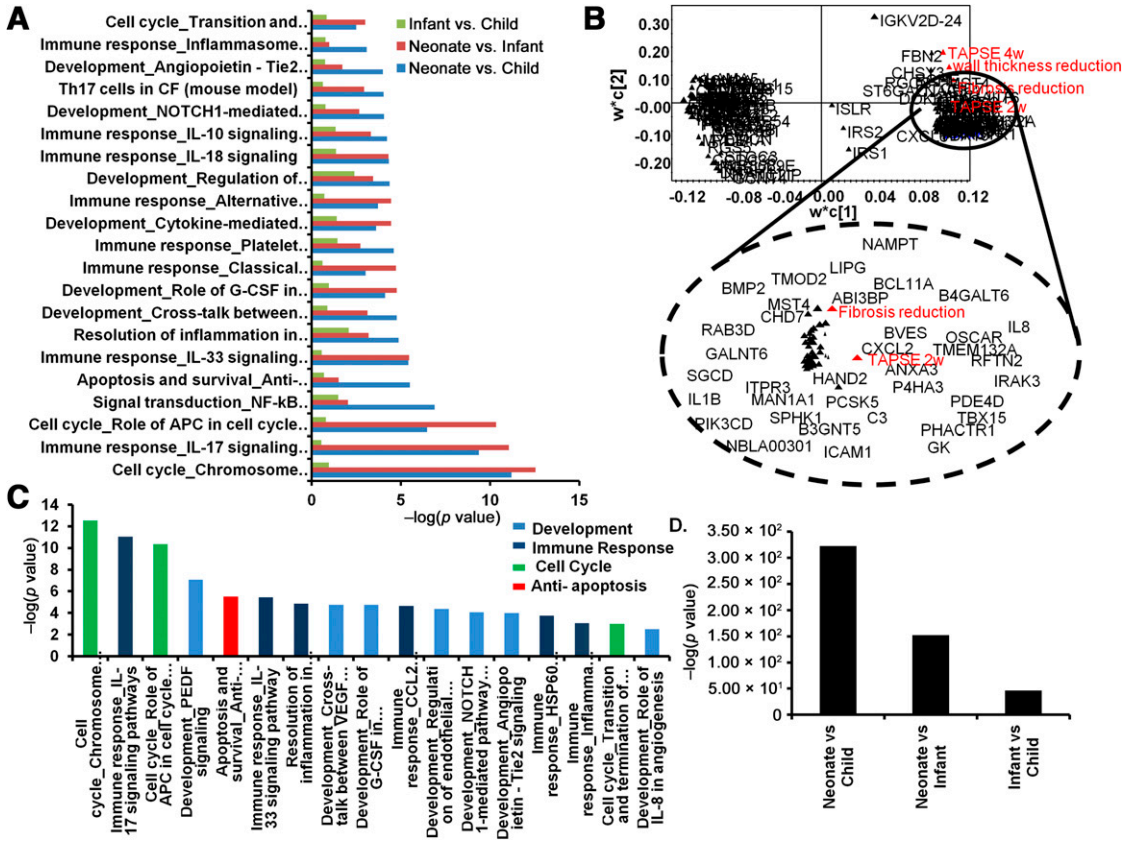

Figure 5. Computational modeling and systems biology. **(A):** Gene pathway analysis. Complete pathway analysis of all genes that were changed. All three groups were compared with each other, neonate versus child (blue), neonate versus infant (red), and infant versus child (green) (n = 3 in each group). Data show some pathways that were conserved between neonates and infants (where red and blue or red and green are similar), as well as some that differ between all three. **(B):** Partial least squares regression (PLSR) analysis of gene array. The top 300 genes were plotted in principal component space using PLSR analysis. Enlarged inset demonstrates the cluster of genes that localized at the same space with the function of TAPSE, fibrosis, and hypertrophy. Note the presence of important cardiac genes (such as *hand2*, *nmp2*, and *cxcl2*) and cytokines (IL8 and IL1B). PLSR analysis does not indicate the direction of the change, merely which ones are contributing to the response (positively and negatively). **(C):** Pathway analysis. Based on gene expression analysis, upregulated pathways were compared between neonate and child groups. **(D):** Enrichments. PLSR identified the top 300 altered genes contributing to the responses, with most significant enrichment observed in the neonate-versus-child comparison. Abbreviation: TAPSE, tricuspid annular plane systolic excursion.

selecting miRNAs with validated targets, we also ran pathway analysis on those targets (Fig. 4C) and found pathways similar to those of our gene analysis. We ran the miRNA and gene arrays on three patients from each group. Although the ages were similar in the groups, the diagnoses and genders of the patients were different. We excluded any patient with known genetic mutations; however, many of these patients may have unknown genetic underlying causes and our study did not account for that. To counter these issues, more patient samples need to be added to perform multivariate analysis; because of the low prevalence of CHDs, it will take time to gather enough samples to account for these other variables. Finally, our data also demonstrated that all individual cell lines may not grow at the same rate, leaving the possibility that a given patient could be over-represented in the pooled sample (data not shown). Although this could be a concern, pooled lines also proliferated differently than the sum of the individual lines, indicating that the cells may behave differently when pooled. As our ability to collect more patient cells increases over time, we will be able to examine patient-to-patient variability in many parameters.

Pathway analysis of gene array data demonstrated that genes responsible for cell-cycle regulation, development, angiogenesis, anti-inflammatory response, regeneration, and anti-apoptosis were upregulated in neonatal cells compared with infant or child hCPCs. Interestingly, collagen IV was decreased in neonate cells, and many pro-stem cell homing factors were enriched. Full pathway analysis of all 3 groups is shown in Figure 5A, as well as full PLSR to identify genes that mapped to function (Fig. 5B). These data need to be validated in future studies but present interesting mechanistic insights, some of which were validated by our in vitro and in vivo studies.

We further analyzed some of the pathways based on our observations from computational modeling. One of the observations was the preservation of the pathways responsible for angiogenesis among all ages of hCPCs. CPCs are known to have an increased angiogenic potential [19, 20]. In fact, recently the regenerative capacity of CPCs has been attributed to their capacity to form vessels and not cardiac myocytes [21, 22]. In corroboration with the literature as well as the pathways suggested by our computational modeling, we observed increased vessel formation among all the different age groups of hCPCs.

From the potential mechanisms based on our computational biology approach, we also observed increased expression of miRNAs and genes in neonatal hCPCs involved in cell cycle and proliferation pathways. Our proliferation assay data suggest that neonates

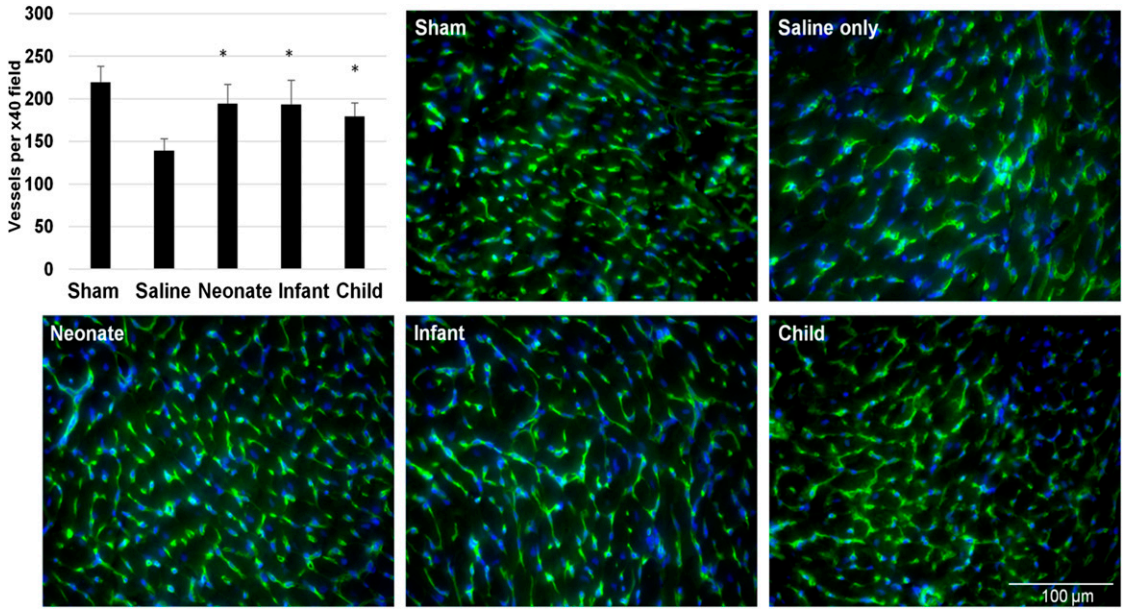

Figure 6. Angiogenesis analysis. Isolectin staining and quantification was performed. Vessels were quantified by counting the total number of vessels per unit area. Three cross-sectional areas from right ventricles of each animal were quantified. Human cardiac progenitor cells from each age group (neonate, infant, and child; n = 4 rats per group) showed significantly increased angiogenesis. *, $p < .05$; analysis of variance followed by Tukey-Kramer post-test.

have the maximum capacity to proliferate, implying that donor age is a major factor in proliferative potential. We also observed increased expression of genes and miRNAs involved in stem cell homing in neonatal cells compared with infant or child hCPCs. Also, the literature suggests that CPCs have an increased ability to attract c-kit-positive cells [23], MSCs, and other cell types [24] to the site of injury. Based on these observations, we performed a migration assay using hCPC conditioned media with human MSCs in a modified Boyden chamber assay. Our data demonstrate an increased ability of neonates to attract MSCs, followed by infant and child. To assess this further, we performed immunostaining of nondonor c-kit-positive cells and SCA-1-positive cells in the RV musculature. Although the numbers were too few to accurately quantify, our images suggest recruitment of more endogenous c-kit-positive and SCA-1-positive cells in the rats treated with neonate CPCs compared with other age groups, suggesting that these cell types have more capacity to attract other cell types toward the site of injury (supplemental online Fig. 1; Fig. 7C). Furthermore, recruitment of SCA-1-positive cells in the right ventricle suggests the role these cells might play in the findings observed after 2 weeks of cell transplantation. c-kit-positive CSCs are known to attract SCA-1-positive cells [25]. Whether these cells play a role in improved RV remodeling is still a subject of study. However, based on the current literature, SCA-1 has been identified on various stem/precursor cell types, including hematopoietic, mesenchymal, and endothelial progenitor cells, and plays a role in regeneration and apoptosis, therefore improving ventricular remodeling.

To demonstrate the fate of the implanted hCPCs, we performed immunostaining for human mitochondria antigen together with c-kit, cardiac troponin, or von Willebrand factor (data not shown). Although our in vivo imaging data demonstrated that at day 21 <20% of the initial DiR signal was retained in right ventricle, we could not observe any staining of human mitochondria or human nuclear antigen in the rat heart on tissue isolated at day 28. Similar results have been reported in the literature, where various groups have used various cell tracking methods and have observed almost negligible signal after 3–5 weeks of cell implantation [26–28]. Whereas it is possible that DiR was lost over time, we have used this technique in the past to track cells successfully. Additionally, whereas it is possible that DiR was not passed to daughter cells, we were unable to see large amounts of c-kit-positive cells of any type in the right ventricle. We looked at cells at an earlier time point (7 days) and saw no differences in the presence of implanted cells, nor were we able to see differences in costaining with mature markers. Taken together, these results point toward the importance of paracrine-based regenerative effects of c-kit-positive hCPCs.

Our data add to the growing body of literature involving regeneration of RV myocardium in patients with congenital heart diseases. Recently, scientists have demonstrated improved remodeling of right ventricle after delivery of umbilical vein mononuclear cells in a mouse model of RV failure [29]. The study reported that these cell types work by decreasing fibrosis and increasing cell proliferation, similar to our study. The group further tested the viability of their approach in right ventricle of juvenile porcine model to assess its safety [29]. Another phase I clinical trial involving intracoronary delivery of human pediatric cardiosphere cells in patients with hypoplastic left heart syndrome suggested the beneficial role these cells play in improved cardiac remodeling. That trial included a pediatric patient population of varied ages (neonate to ≥ 3 years) and used autologous cardiosphere-derived cells [9, 15].

Our study is a step forward to further refine these observations by analyzing the role of CPC age in improved remodeling in RV heart failure. Our computational biology approach suggests newer mechanisms that still need to be deciphered for a better understanding of these cell types. In fact, after initial computational modeling predicted pathways that were validated by in vitro studies, we added these outputs to create an updated model (data not shown) with new inputs. Interestingly, the incorporation of new outputs did not alter the importance of any miRNAs,

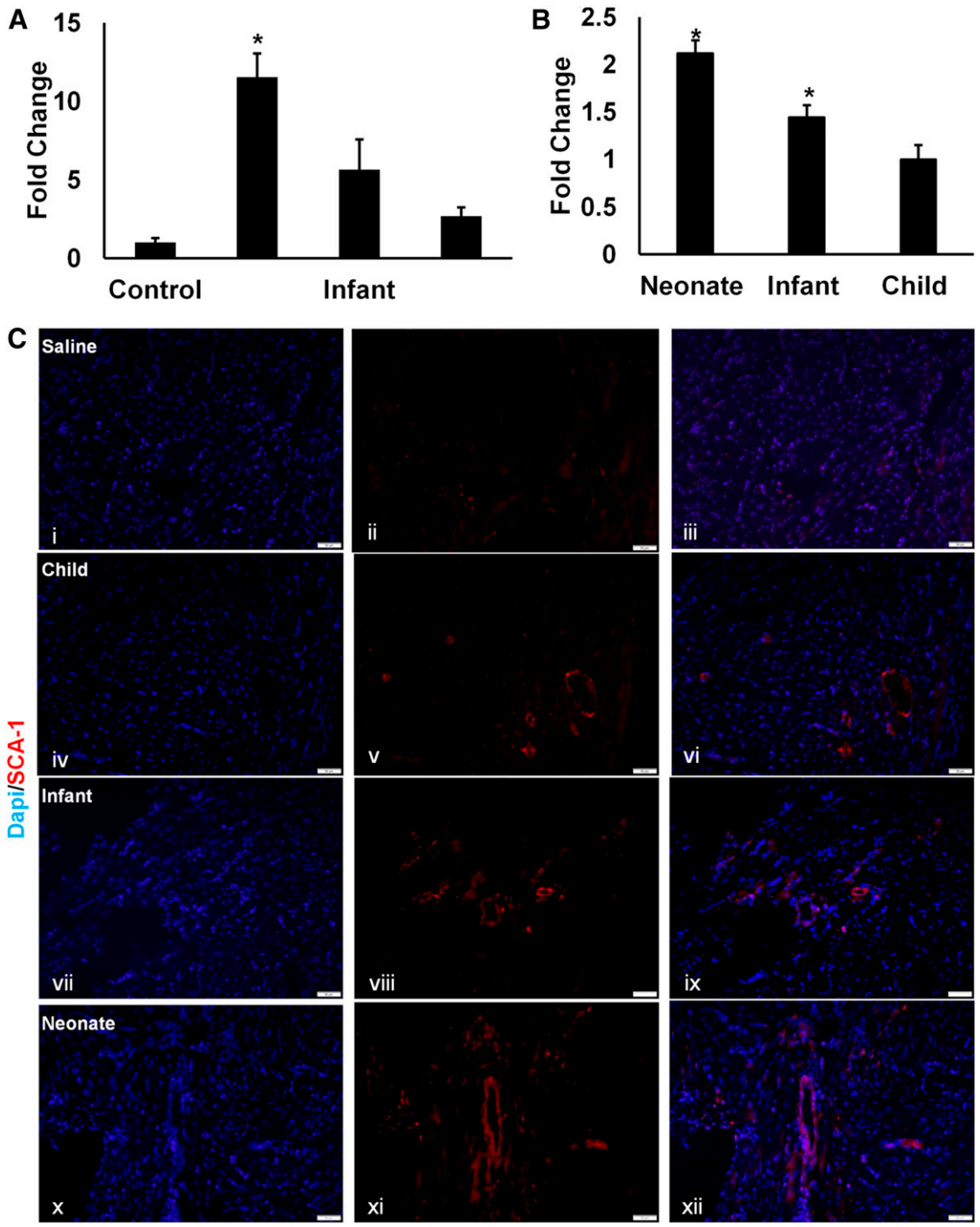

Figure 7. Chemotaxis and proliferation. **(A):** Migration assay. Medium from neonatal human cardiac progenitor cells (hCPCs) induces migration of mesenchymal stem cells (MSCs). Human MSCs were incubated in a modified Boyden chamber assay for 18 hours in the presence of control media (no serum Dulbecco's modified Eagle's medium) or serum-free media from neonatal, infant, and child hCPCs. The top filter was swabbed, and the migrated cells were stained with DAPI and counted. Treatment media from neonate hCPCs showed significantly increased migration of human MSCs ($n = 3$). $*$, $p < .05$; analysis of variance (ANOVA) followed by Tukey-Kramer post-test. **(B):** Proliferation assay. Absorbance was calculated after incubation of 10,000 cells from each group for 24 hours with 5-ethynyl-2′-deoxyuridine for 3 contiguous passages. Neonate hCPCs showed significantly increased proliferative ability compared with other cell types. $*$, $p < .05$; ANOVA followed by Tukey-Kramer post-test. **(C):** SCA-1 immunostaining. Chemotactic ability of the transplanted cells was confirmed by performing SCA-1 in vivo immunostaining 7 days after transplantation of the cells. Representative images of SCA-1-positive cells in right ventricular wall of cell transplanted animals with c-kit-positive CSCs (iv–xii) compared with saline-only controls (i–iii). Blue, DAPI; red, SCA-1. Error bars, 75 μm. Abbreviations: Dapi, 4′,6-diamidino-2-phenylindole; SCA, stem cell antigen.

both showing the robustness of the model and adding potential new miRNA-output relationships to further test. Although no miRs or genes were directly shown to be involved, this type of modeling can also show covarying miRNAs as we have done in the past, further strengthening the role of computational modeling in predicting responses.

Acknowledgments

This work was supported by Grant HL124380 from the National Heart, Lung, and Blood Institute to M.E.D. and M.O.P., funds from the Center for Pediatric Nanomedicine at Children's Healthcare of Atlanta, and the Darryll M. Ceccoli Research Fund with thanks to Katrina Ceccoli. Research reported in this publication was also supported by the National Heart, Lung, and Blood Institute under award T32HL007745.

Author Contributions

U.A.: conception and design, performance of research, data analysis and interpretation, manuscript writing, final approval of manuscript; A.W.S.: conception and design, performance of research, data analysis and interpretation; K.M.F., A.V.B., A.G., D.T., M.E.B., and M.S.: performance of research; R.J.: performance of research, data analysis and interpretation; J.D.F., B.E.K., K.R.K., and B.A.: provision of study material or patients; M.B.W.: conception and design, manuscript writing; M.O.P.: data analysis and interpretation; M.E.D.: conception and design, data analysis and interpretation, manuscript writing, final approval of manuscript.

Disclosure of Potential Conflicts of Interest

The authors indicated no potential conflicts of interest.

References

1 Bolli R, Chugh AR, D'Amario D et al. Cardiac stem cells in patients with ischaemic cardiomyopathy (SCIPIO): Initial results of a randomised phase 1 trial. Lancet 2011;378:1847–1857.

2 Makkar RR, Smith RR, Cheng K et al. Intracoronary cardiosphere-derived cells for heart regeneration after myocardial infarction (CADUCEUS): A prospective, randomised phase 1 trial. Lancet 2012;379:895–904.

3 Bergmane I, Lacis A, Lubaua I et al. Follow-up of the patients after stem cell transplantation for pediatric dilated cardiomyopathy. Pediatr Transplant 2013;17:266–270.

4 Rychik J, Goldberg DJ. Late consequences of the Fontan operation. Circulation 2014;130: 1525–1528.

5 Voelkel NF, Quaife RA, Leinwand LA et al. Right ventricular function and failure: Report of a National Heart, Lung, and Blood Institute working group on cellular and molecular mechanisms of right heart failure. Circulation 2006; 114:1883–1891.

6 Beltrami AP, Barlucchi L, Torella D et al. Adult cardiac stem cells are multipotent and support myocardial regeneration. Cell 2003;114:763–776.

7 Nadal-Ginard B, Kajstura J, Leri A et al. Myocyte death, growth, and regeneration in cardiac hypertrophy and failure. Circ Res 2003;92: 139–150.

8 Oommen S, Yamada S, Cantero Peral S et al. Human umbilical cord blood-derived mononuclear cells improve murine ventricular function upon intramyocardial delivery in right ventricular chronic pressure overload. Stem Cell Res Ther 2015;6:50.

9 Ishigami S, Ohtsuki S, Tarui S et al. Intracoronary autologous cardiac progenitor cell transfer in patients with hypoplastic left heart syndrome: The TICAP prospective phase 1 controlled trial. Circ Res 2015;116:653–664.

10 Bergmann O, Bhardwaj RD, Bernard S et al. Evidence for cardiomyocyte renewal in humans. Science 2009;324:98–102.

11 Ye J, Hom DS, Hwang J et al. Aging impairs the proliferative capacity of cardiospheres, cardiac progenitor cells and cardiac fibroblasts: Implications for cell therapy. J Clin Med 2013;2:103–114.

12 Capogrossi MC. Cardiac stem cells fail with aging: A new mechanism for the age-dependent decline in cardiac function. Circ Res 2004;94: 411–413.

13 Simpson DL, Mishra R, Sharma S et al. A strong regenerative ability of cardiac stem cells derived from neonatal hearts. Circulation 2012; 126(suppl 1):S46–S53.

14 Ishigami S, Ohtsuki S, Tarui S et al. Intracoronary autologous cardiac progenitor cell transfer in patients with hypoplastic left heart syndrome (TICAP): A prospective phase 1 controlled trial. Circ Res 2015;116:653–664.

15 Tarui S, Ishigami S, Ousaka D et al. Transcoronary infusion of cardiac progenitor cells in hypoplastic left heart syndrome: Three-year follow-up of the Transcoronary Infusion of Cardiac Progenitor Cells in Patients With Single-Ventricle Physiology (TICAP) trial. J Thorac Cardiovasc Surg 2015;150: 1198–1207, 1208.e1–1208.e2.

16 Gray WD, French KM, Ghosh-Choudhary S et al. Identification of therapeutic covariant microRNA clusters in hypoxia-treated cardiac progenitor cell exosomes using systems biology. Circ Res 2015;116:255–263.

17 Dong D-l, Yang B-f. Role of microRNAs in cardiac hypertrophy, myocardial fibrosis and heart failure. Acta Pharm Sin B 2011;1:1–7.

18 Krane M, Deutsch MA, Doppler S et al. Small RNAs make big impact in cardiac repair. Circ Res 2015;116:393–395.

19 Kajstura J, Urbanek K, Rota M et al. Cardiac stem cells and myocardial disease. J Mol Cell Cardiol 2008;45:505–513.

20 Davis DR, Ruckdeschel Smith R, Marbán E. Human cardiospheres are a source of stem cells with cardiomyogenic potential. Stem Cells 2010;28:903–904.

21 van Berlo JH, Molkentin JD. An emerging consensus on cardiac regeneration. Nat Med 2014;20:1386–1393.

22 van Berlo JH, Kanisicak O, Maillet M et al. c-kit+ cells minimally contribute cardiomyocytes to the heart. Nature 2014;509:337–341.

23 Chen Z, Pan X, Yao Y et al. Epigenetic regulation of cardiac progenitor cells marker c-kit by stromal cell derived factor-1α. PLoS One 2013;8:e69134.

24 Li TS, Suzuki R, Ueda K et al. Analysis of the origin and population dynamics of cardiac progenitor cells in a donor heart model. Stem Cells 2007;25:911–917.

25 Liu J, Wang Y, Du W et al. Sca-1-positive cardiac stem cell migration in a cardiac infarction model. Inflammation 2013;36:738–749.

26 Hong KU, Guo Y, Li QH et al. c-kit+ Cardiac stem cells alleviate post-myocardial infarction left ventricular dysfunction despite poor engraftment and negligible retention in the recipient heart. PLoS One 2014;9:e96725.

27 Hong KU, Li QH, Guo Y et al. A highly sensitive and accurate method to quantify absolute numbers of c-kit+ cardiac stem cells following transplantation in mice. Basic Res Cardiol 2013; 108:346.

28 Terrovitis J, Stuber M, Youssef A et al. Magnetic resonance imaging overestimates ferumoxide-labeled stem cell survival after transplantation in the heart. Circulation 2008;117:1555–1562.

29 Cantero Peral S, Burkhart HM, Oommen S et al. Safety and feasibility for pediatric cardiac regeneration using epicardial delivery of autologous umbilical cord blood-derived mononuclear cells established in a porcine model system. Stem Cells Translational Medicine 2015;4:195–206.

See www.StemCellsTM.com for supporting information available online.